Chapter 2

Local Loops and Their Measurement Setup

2.1 Introduction

The system identification process generally consists of three entities [18]:

1. A data set, the input to the process.
2. A model structure, a relationship between the data set and model parameters.
3. A method of identification.

The first two entities, data set and model structure, are the main focus of this chapter. They are the most important foundations of the identification algorithm development. The first phase of the system identification algorithm development is to gain all *a priori* knowledge on the subject under identification. Such knowledge includes models, simulations, and/or the general behavior of the subject.

Our identification subject is the telephone subscriber loop and its measurement environment. In this chapter, the subject is studied in four stages:

- Modeling of Twisted Pairs (TPs) (Section 2.2).
- Modeling of Local Loop Structures (Section 2.3).
- Modeling and Simulation of Loop Measurements (Sections 2.4 and 2.5).
- Analysis of Transmission Line Behavior (Section 2.6).

The subscriber loop can be viewed as a transmission line network for a telecommunication system, and its signal propagation behavior is completely characterized by transmission line theory [5], [4]. The subscriber loop's transmission medium, or the twisted pair (TP) segments, has been modeled within the context of transmission line theory [19]. The local loop topology — how TPs are connected — is modeled as a graph. With the TP and loop topology models, the measurement setup is modeled accordingly. With the Thevenin impedance of a subscriber loop, the measurement input-output

characteristic is modeled as a simple voltage-divider equivalent circuit. Lastly, the analysis of the behavior of a transmission line is presented using a bounce diagram and a system block diagram.

2.2 Twisted-Pair Model

The TP type, which is a descriptive parameter specifying the physical characteristics (*e.g.*, wire gauges, cable insulation, and operation temperature) cannot be associated directly with the loop measurement, which is a strictly numeric quantity . Instead, the TP type needs to be converted into its electrical characteristics, specifically the well-known transmission line characteristic impedance $Z_0(f)$ [Ω] and propagation function $\gamma(f)$ [7], [8], [5], [4]. The characteristic impedance is the ratio of the voltage to the current traveling in an infinitely long TP (no returning signal). The real and imaginary parts of the propagation function are the attenuation function $\alpha(f)$ [Np/m] and phase function $\beta(f)$ [rad/m] of the TP. The attenuation and phase functions express the amount of signal attenuation and phase shift, respectively, that occurs by traveling through a unit length of the TP. Furthermore, transmission lines are often modeled with a lumped circuit model for a unit length, as shown in Figure 2-1. The $R'(f)$, $L'(f)$, $C'(f)$, $G'(f)$ (collectively referred to as the RLCG parameters) are defined as resistance per unit length (in Ω/m), inductance per unit length (in H/m), capacitance per unit length (in F/m), and conductance per unit length (in Siemens/m or S/m), respectively. The relationships between the RLCG parameters and $Z_0(f)$ and $\gamma(f)$ are

$$Z_0(f) = \sqrt{\frac{R'(f) + j2\pi f L'(f)}{G'(f) + j2\pi f C'(f)}} \tag{2-1}$$

and

$$\gamma(f) = \alpha(f) + j\beta(f) = \sqrt{\left(R'(f) + j2\pi f L'(f)\right)\left(G'(f) + j2\pi f C'(f)\right)}\,. \tag{2-2}$$

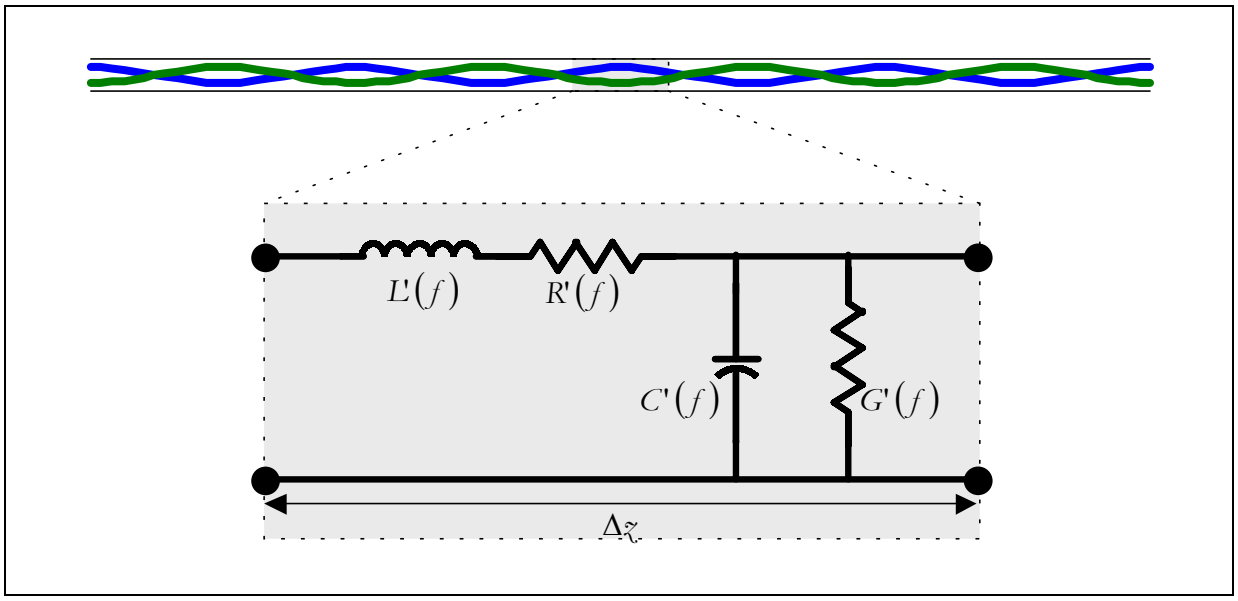

Figure 2-1: Equivalent lumped RLCG circuit of a unit length of twisted-pair transmission line.

There are several kinds of RLCG parameter equations for the available TPs [6], [19]. Some of the analytical models are only valid over a limited frequency range. The VT-TDL TP RLCG model [19], which shows causal behavior and is a good match with the measured RLCG values, is used in this thesis. The parameters for the VT-TDL model are defined as follows:

$$R'(f) = \frac{2\,D/d}{\sqrt{(D/d)^2 - 1}} \operatorname{Re}\{Z_i(f)\}, \tag{2-3}$$

$$L'(f) = T_{ind}\,\frac{\mu_0}{\pi}\cosh^{-1}\left(\frac{D}{d}\right) + \frac{D/d}{\pi f\sqrt{(D/d)^2 - 1}} \operatorname{Im}\{Z_i(f)\}, \tag{2-4}$$

$$C'(f) = \frac{\pi\varepsilon_r\varepsilon_0}{\cosh^{-1}(D/d)}, \tag{2-5}$$

and,

$$G'(f) = 0\,. \tag{2-6}$$

where D is the center-spacing between the two wires (in meters), d is the diameter of the conductor (in meters), μ_0 is the permeability of air ($4\pi\times10^{-7}$ m/s), T_{ind} is the twisting index, ε_0 is the permittivity of air (~8.854×10^{-12} F/m), and ε_r is the relative permittivity or dielectric constant of the insulation. The internal impedance $Z_i(f)$ is defined as

$$Z_i(f) = \frac{1}{d}\sqrt{\frac{2f\mu_0}{j\pi\sigma}}\frac{J_0\left(d\sqrt{(\pi\mu_0\sigma/2j)f}\right)}{J_1\left(d\sqrt{(\pi\mu_0\sigma/2j)f}\right)} \tag{2-7}$$

where σ is the conductivity of the conductor (in siemens/meter), and $J_n(x)$ is the Bessel function of the first kind of order n.

The parameters for the TP types under consideration are shown in Table 2-1. These TP types are based on 22, 24, and 26 AWG PIC TPs at 21 °C as tabulated in the ANSI T1.601-1999 Standard [10] as mentioned in Chapter 1, and their corresponding parameters are obtained by fitting the model in a least-squares sense. A database of the parameters for all descriptive TP types under consideration should be made available for the conversion from a descriptive TP physical type to its corresponding electrical characteristics. This will provide data for the loop simulation and identification.

Table 2-1: Parameters for the VT-TDL TP RLCG for selected TP types. All are PIC TP at 21 °C.

	22 AWG	24 AWG	26 AWG
d [mm]	0.91010s	0.67746	0.47911
D [mm]	1.1364	0.85103	0.60652
σ [S/m]	4.7472×10^7	5.3256×10^7	6.0413×10^7
T_{ind}	1.5968	1.5758	1.5512
ε_r	1.2819	1.3004	1.3239

2.3 Structural Modeling of a Local Loop

The structure of the loop-under-identification (LUI) is modeled as a graph [20] in Figure 2-2. Vertices of the graph are referred to as loop nodes, and the graph's edges represent the TP segments. Each vertex of the graph is numbered with simple Arabic integers and each edge is numbered with circled Arabic integers. The loop nodes and TP segments are referred as "Node #" and "Segment #" with their corresponding vertex and edge numbers. The graph is always connected and acyclic (that is, there exists one and only one path from any loop node to any other node). Moreover, the loop nodes

are classified into three types — Termination, Gauge Change (GC), and Bridged Tap (BT) — in accordance with the number of TPs attached, as indicated in Figure 2-2.

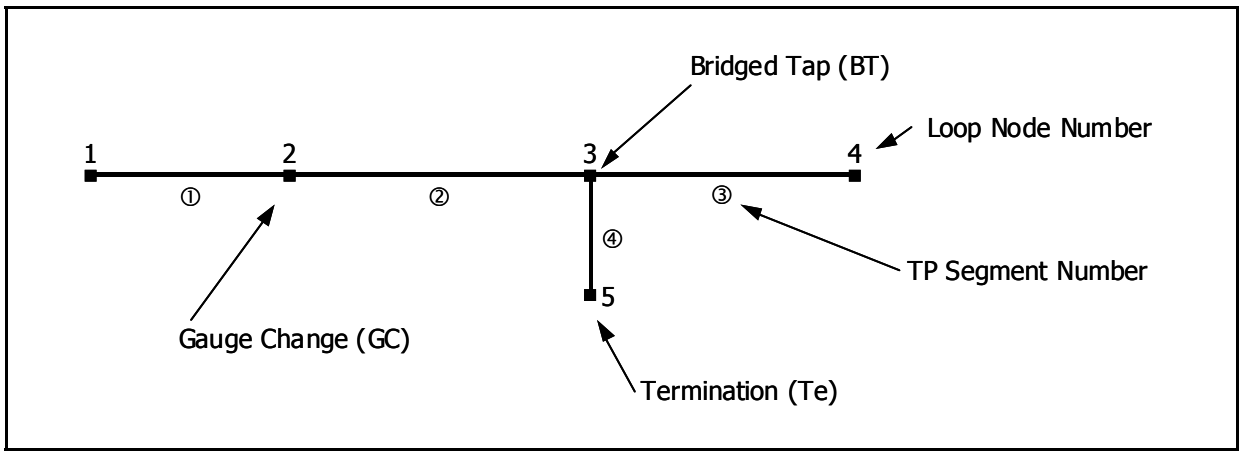

Figure 2-2: Graph representation of subscriber line.

While each TP segment (edge of the graph) contains both TP type and length parameters, there are no parameters associated with the loop node. The loop nodes are equivalent to either the distribution cabinets or splice cases on the subscriber line, and the inclusion of such non-ideal connection points in the model is introduces discrepancies in the loop's overall characteristics. However, for the sake of simplicity, we assume that ideal TP connections are made in these cabinets (and cases). Furthermore, all nodes are assumed to be electrically unterminated — that is, open circuit to ground. This assumption entails the other assumption that the subscriber is not connected to the loop, and consequently locating the subscriber node is not within the scope of this thesis.

2.4 Modeling of the Local Loop Measurement Setup

The above two sections present models for TP characteristics and loop structures that are independent of the measurement environment. This section defines the model for the overall measurement environment as a linear time-invariant (LTI) system with the excitation signal as its input and the response as its output. The LTI system is described in terms of its frequency response. The response is obtained through the LUI's Thevenin impedance and a simple voltage divider circuit.

Figure 2-3 is a simplified diagram showing a single-port loop measurement hook-up. The LUI is connected to a measurement device (which in its simplest form is a voltage source and a voltmeter) with an interface — a balun — to obtain a balanced measurement. The input and measured signals

are denoted as $x(t)$ and $y(t)$, respectively. The source impedance Z_g is assumed to be purely resistive and is set to 120 Ω to roughly match the typical TP characteristic impedance.

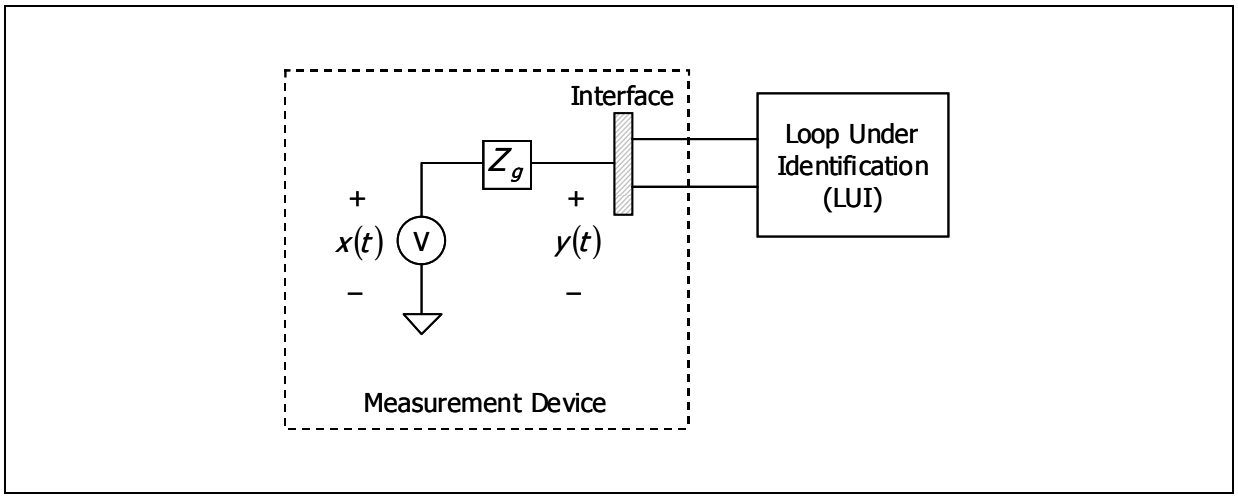

Figure 2-3: Loop measurement setup.

While the graph representation of the LUI provides the complete structural model for the local loop, it is not yet directly related to any measurable quantity. Given the knowledge of the TP electrical characteristics and that the loops are linear and time-invariant (LTI) systems, the measurement setup in Figure 2-3 can be modeled as an LTI system with frequency response $H(f)$, as illustrated in Figure 2-4(a), with $x(t)$ as input and $y(t)$ as output. The important property is that the input-output behavior of a bounded-input-bounded-output (BIBO) stable LTI system can be completely described by its frequency response $H(f)$.

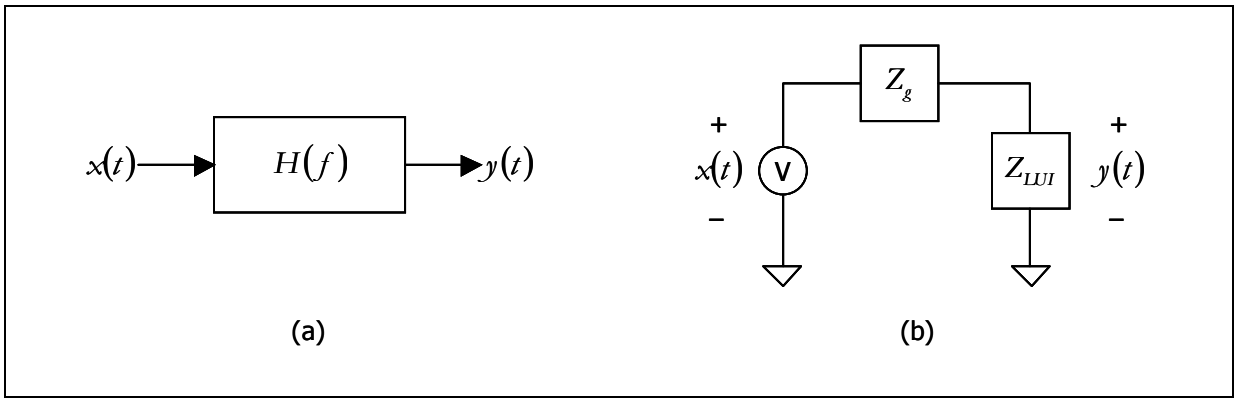

Figure 2-4: LTI System (a) and voltage divider circuit (b) representations of TP loop measurement setup.

Moreover, this system can be seen as a voltage divider circuit shown in Figure 2-4(b), or represented by

$$H(f) = \frac{Y(f)}{X(f)} = \frac{Z_{LUI}(f)}{Z_g + Z_{LUI}(f)} \tag{2-8}$$

where $Z_{LUI}(f)$ is the Thevenin impedance, or input impedance, of the LUI; and $X(f)$ and $Y(f)$ are the Fourier transforms of $x(t)$ and $y(t)$, respectively. $Z_{LUI}(f)$ is computed recursively from the far end of the loop. For each TP segment, its input impedance $Z_{TP}(f)$, with length l in meters and load impedance $Z_L(f)$, is computed from [5]

$$Z_{TP}(f) = Z_0(f)\frac{Z_L(f) + Z_0(f)\tanh\gamma(f)l}{Z_0(f) + Z_L(f)\tanh\gamma(f)l}. \tag{2-9}$$

The load impedance $Z_L(f)$ for the far end segment is assumed to be infinite (open circuit), and $Z_L(f)$ for any other segment is the aggregated $Z_{TP}(f)$ of the next segment. $Z_{TP}(f)$ of the near-end segment is then denoted as $Z_{LUI}(f)$.

The simulated frequency responses $H(f)$ for CSA Test Loop #1 (or simply CSA #1) measured at Node 4 and for CSA #4 measured at Node 1 are shown in Figure 2-5 and Figure 2-6, respectively, from 1 kHz to 100 MHz. Although details of the response are always different for different loop structures, the overall trend of the response that is seen in these figures is typical for most loops.

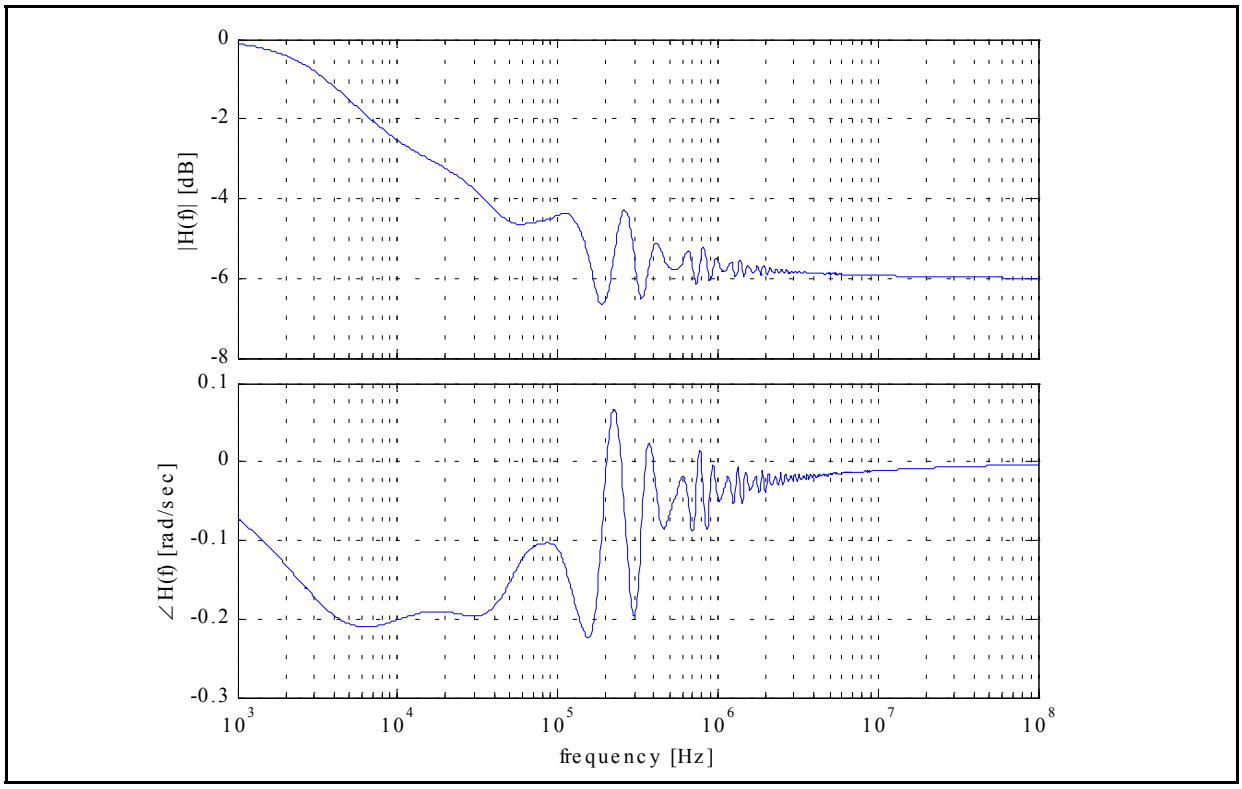

Figure 2-5: Frequency Response of CSA #1 at Node 4.

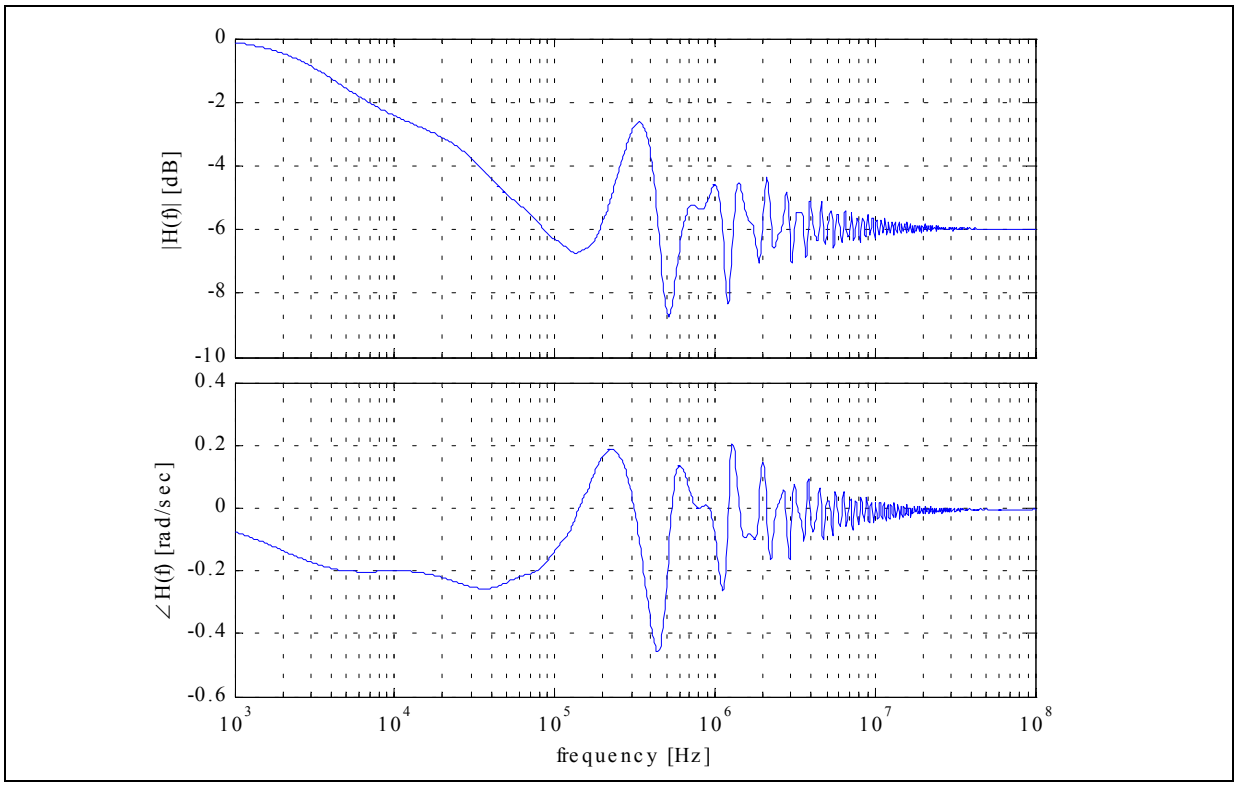

Figure 2-6: Frequency Response of CSA #4 at Node 1.

2.5 Simulating Local Loop Measurements

In this section, the simulations of the two types of LUI measurements used in this thesis, the time domain reflectometry (TDR) response and frequency response, are presented. With the system frequency response $H(f)$ from the previous section, any desired characteristic for the subscriber loop can now be simulated. However, there is a practical limitation due to the wideband nature of the TP loops and the discrete approximations (*i.e.*, aliasing problem) of computer simulation. Hence, the input signal must be bandlimited or at least have sufficient roll-off at higher frequencies.

2.5.1 TDR Response Measurement

The TDR is widely used in the telecommunications industry for multiple tasks such as loop length approximation and bridged tap recognition. Basically, the TDR instrument consists of a variable pulse generator and an oscilloscope for the display of the response. The TDR is the transmission line counterpart to sonar for underwater objects and radar for mid-air objects. The TDR response consists of reflections returning from transmission line discontinuities down the line. Moreover, the response provides intuition for the location of transmission line discontinuities or abnormalities. In the context of the subscriber line structural model, each TDR reflection pulse corresponds to a loop node.

To simulate TDR responses, we have elected to make the input signal a raised-cosine (or Hanning) pulse:

$$x_{TDR}(t) = \frac{A}{2}\left[1 - \cos\left(\frac{2\pi t}{T_{PW}} + \pi\right)\right] \tag{2-10}$$

where A and T_{PW} are the pulse amplitude (in volts) and width (in seconds), respectively. For this thesis, a 10-V 1-μs pulse (as shown in Figure 2-7) will be used as a default TDR input pulse unless otherwise noted.

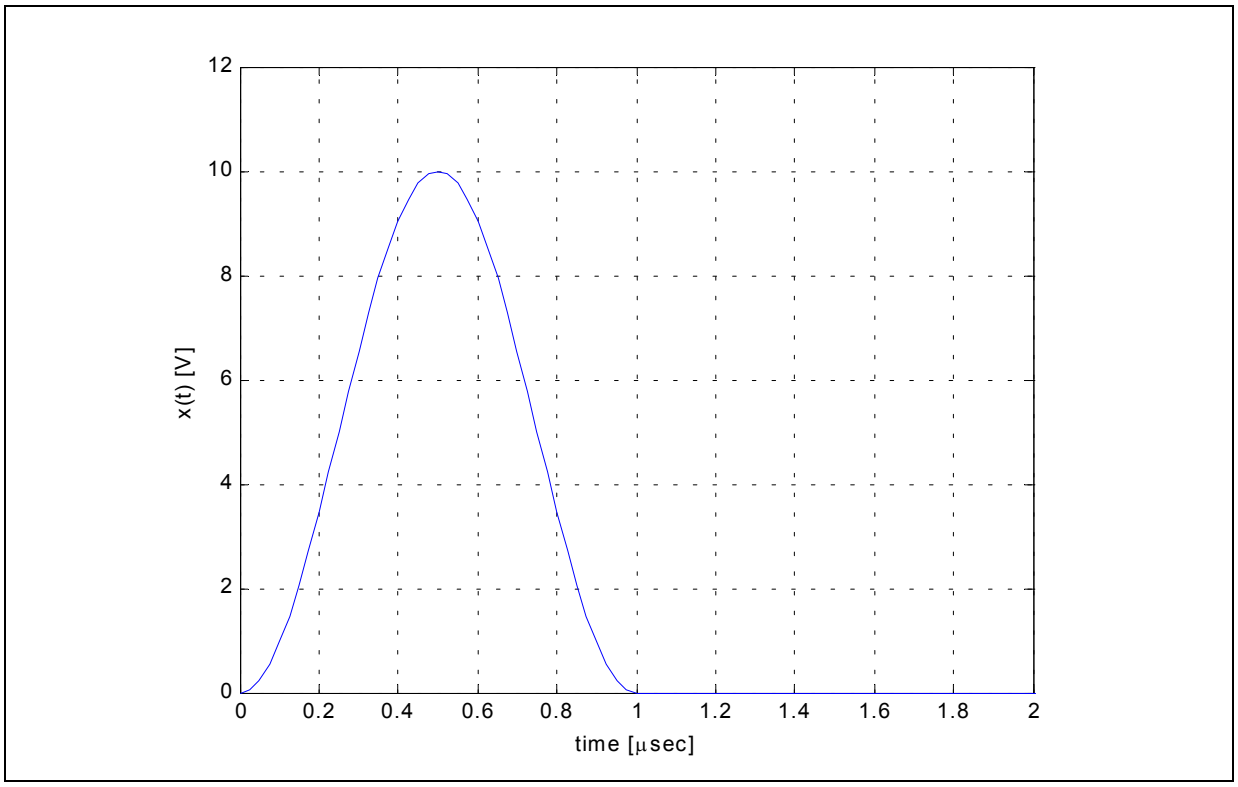

Figure 2-7: TDR input signal example. 10-V 1-μs raised-cosine (Hanning) pulse.

The TDR response $y_{TDR}(t)$ is obtained by convolving $x_{TDR}(t)$ and the system impulse response $h(t)$, or equivalently in the frequency domain:

$$Y_{TDR}(f) = X_{TDR}(f)H(f) \tag{2-11}$$

where $X_{TDR}(f)$ and $Y_{TDR}(f)$ are the continuous-time Fourier transforms of the TDR input pulse and response, respectively. In computer simulation, the continuous-time Fourier transform operation is approximated using the discrete Fourier transform (DFT). For illustration the TDR responses CSA #1 from Node 4 and CSA #4 from Node 1 are used again as examples for the TDR response. The raised-cosine input pulse shown in Figure 2-7 is used as input. The responses are sampled at 40 MHz, and the first 20 μs of the response is shown in Figure 2-8 for CSA #1 and in Figure 2-9 for CSA #4. The actual simulation process used a 120 MHz sampling frequency and a pair of 32,768-point fast DFT and fast inverse DFT (FFT and IFFT, respectively) to minimize the effects of both frequency-domain and time-domain aliasing. Sampling of $x_{TDR}(t)$ — continuous not-bandlimited signal — causes the frequency-domain aliasing.

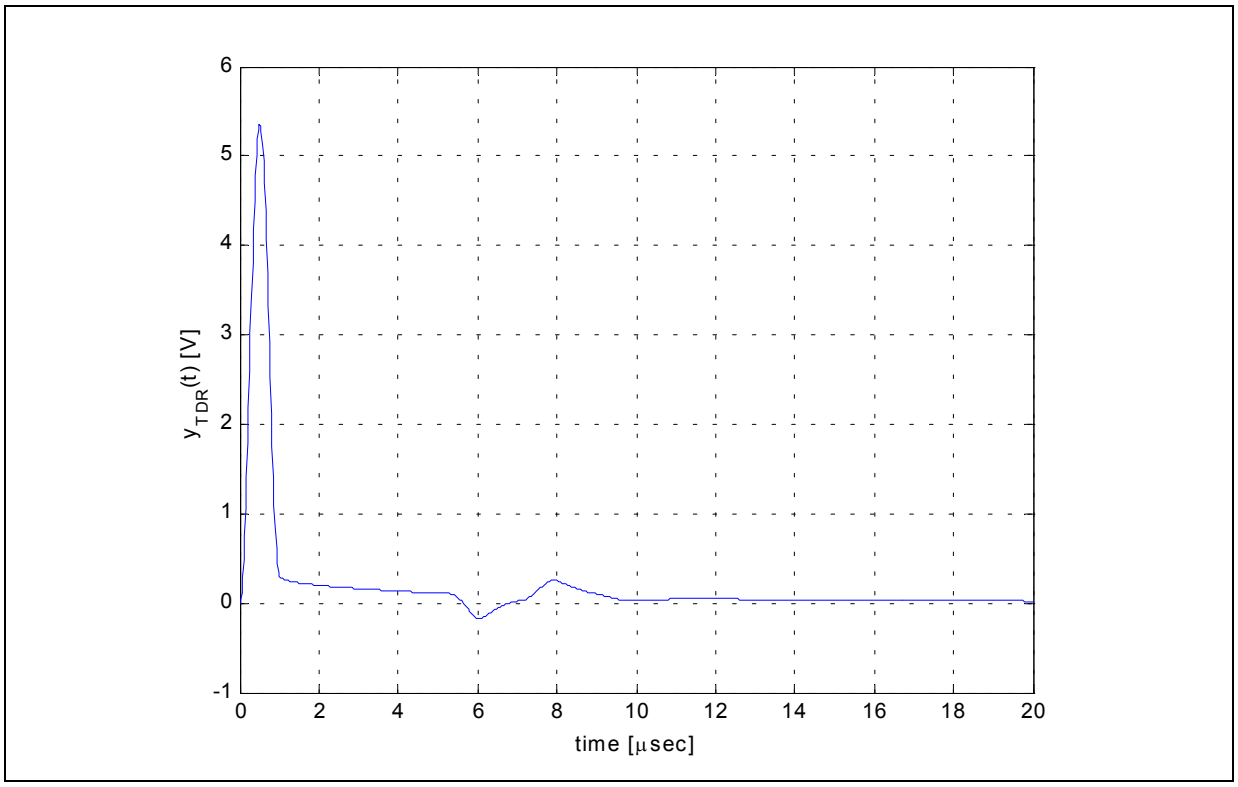

Figure 2-8: TDR response of CSA #1 Loop from Node 4.

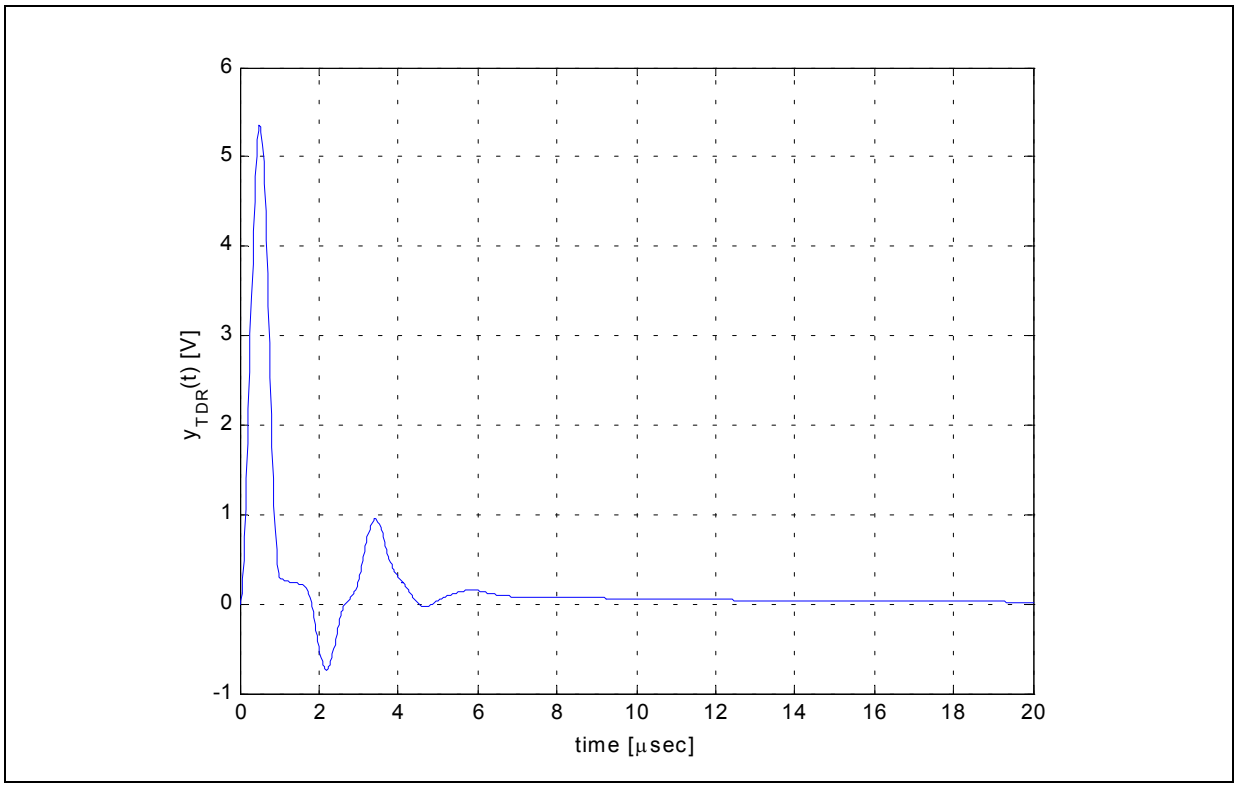

Figure 2-9: TDR response of CSA #4 loop from Node 1.

2.5.2 Frequency Response Measurement

The frequency response measurement $H_M(f_k)$ — which is used in the second identification algorithm in Chapter 5 — can be obtained from a set of sinusoid magnitude and phase measurements at a corresponding set of measurement frequencies $f_k \in M_f$. The ideal measurement is a sampled version of the actual loop frequency response $H(f)$. Unlike the TDR response, which is in the time domain, simulation of the frequency response measurement is achieved simply by computing the frequency response at desired frequency points, and does not require time-consuming FFT operations.

2.6 Analysis of a Transmission Line System

Although Section 2.5.1 mentioned that the TDR response can be related to the location of loop nodes — or ultimately the full loop structure — we have not discussed how they are related to each other. This section will explore the connection between the two in the context of transmission line theory. First, the bounce (or reflection) diagram is used to understand how a signal reflects at loop discontinuities. Then the idea is generalized as a set of subsystems that constructs the overall system in Figure 2-4(a), and each subsystem is visually depicted in a block diagram.

2.6.1 Bounce Diagram: Signal Reflection at Discontinuities

The behavior of a signal traveling through a network of transmission lines (*e.g.*, a subscriber loop) is categorized into three types:

1. Propagation through the transmission line
2. Reflection at discontinuities
3. Transmission at discontinuities.

The signal propagation through the medium is characterized by the line's propagation function $\gamma(f)$ and the distance that the signal has traveled in the medium. For instance, consider a signal with a spectrum $X_0(f)$ observed at the beginning of a TP with length l. The propagated signal spectrum $X_l(f)$, observed at the end of the TP, is defined by

$$X_l(f) = X_0(f) e^{-\gamma(f) l}. \tag{2-12}$$

Discontinuities, or impedance mismatches, on a transmission line loop are Indicative of the nodes of the loop structure model. The discontinuities can appear at the source connection, at the connection of two unmatched lines (GC), at the connection of three lines (BT), and at the end of the transmission line (Termination). Whenever a signal arrives at any discontinuity, a portion of it reflects and returns through the path it came from, and the rest of the signal transmits over the discontinuity, if possible, and continues propagating through the new medium or is sunk into a load. The unloaded end of a transmission line is the only occasion in which total reflection occurs without any transmission.

The amount of signal that is reflected or transmitted is indicated by the reflection function $\Gamma_{ns}(f)$ and the transmission function $\mathrm{T}_{ns}(f)$ (Greek letter Tau). The first subscript *n* indicates the loop node number and the second indicates the TP line segment over which the signal is approaching the discontinuity. The relationship between the two functions is

$$\mathrm{T}_{ns}(f) = 1 + \Gamma_{ns}(f) \tag{2-13}$$

The reflection and transmission functions are defined as the connected transmission line impedances and source/load impedances. With the TP loop structural assumptions, there are four distinct discontinuity types that can appear in our application, as illustrated in Figure 2-10. Assuming the signal is arriving from Segment 1, $\Gamma_{n1}(f)$ for each case is defined as follows: (node subscript indicates the corresponding figure)

$$\Gamma_{a1}(f) = \frac{Z_{0,1}(f) - Z_g}{Z_{0,1}(f) + Z_g}, \tag{2-14}$$

$$\Gamma_{b1}(f) = 1, \tag{2-15}$$

$$\Gamma_{c1}(f) = \frac{Z_{0,1}(f) - Z_{0,2}(f)}{Z_{0,1}(f) + Z_{0,2}(f)}, \tag{2-16}$$

and

$$\Gamma_{d1}(f) = \frac{Z_{0,1}(f) - Z_{0,2}(f) // Z_{0,3}(f)}{Z_{0,1}(f) + Z_{0,2}(f) // Z_{0,3}(f)}. \tag{2-17}$$

where $Z_1 // Z_2 = Z_1 Z_2 / (Z_1 + Z_2)$.

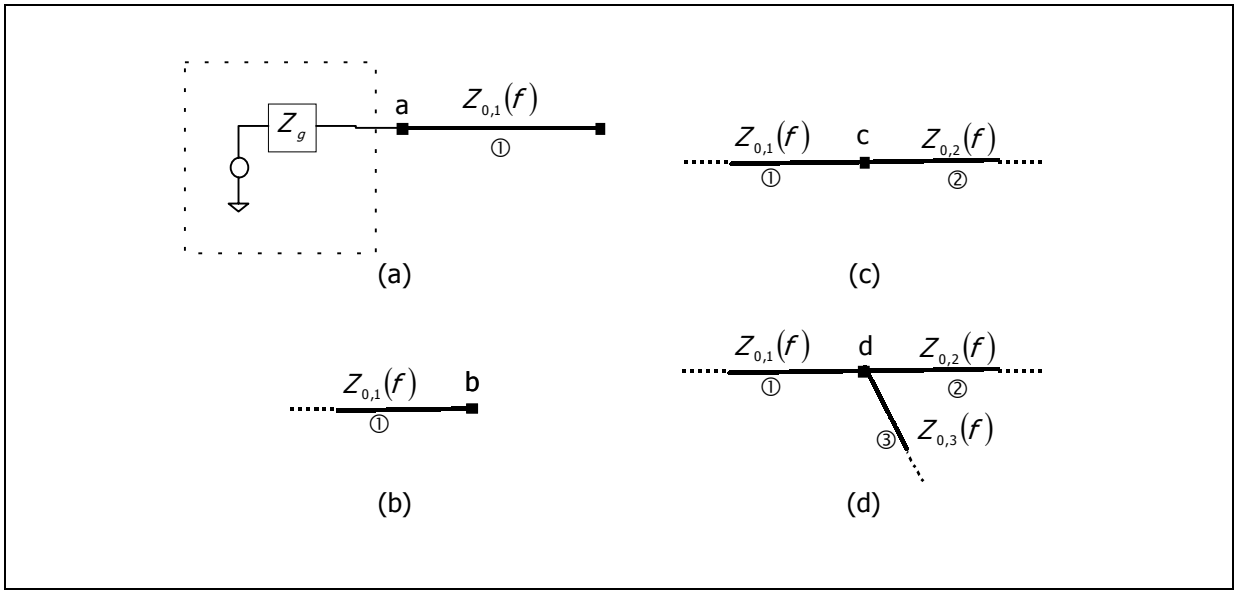

Figure 2-10: TP loop discontinuity possibilities—source-to-loop (a), termination (b), gauge change (c), and bridged tap (d).

To combine all of the above phenomena, the bounce diagram [4], [5] graphically illustrates the signal activity, in both temporal and spatial senses, in a transmission line. A bounce diagram for a simple single-segment TP loop, shown in Figure 2-11, is displayed in Figure 2-12. The distance is on the horizontal axis, and the time is on the vertical axis. The signal excitation from the source enters the loop at time zero and starts propagating through the line. The slope of the plot indicates the propagation velocity of the signal. At time T_1, the signal reaches the end of the segment, and by this time the signal has been attenuated by $e^{-\alpha_1(f)l_1}$. Then, due to the termination of the loop, the signal is completely reflected. After another delay T_1, the signal returns to the source node where only a portion of its energy will be reflected, commensurate with $\Gamma_{11}(f)$. As the signal perpetually bounces back and forth on the loop its strength progressively weakens.

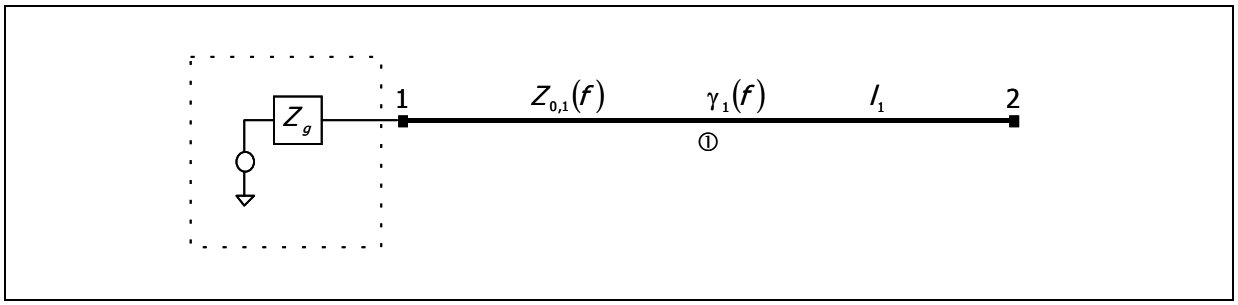

Figure 2-11: Single-segment loop configuration.

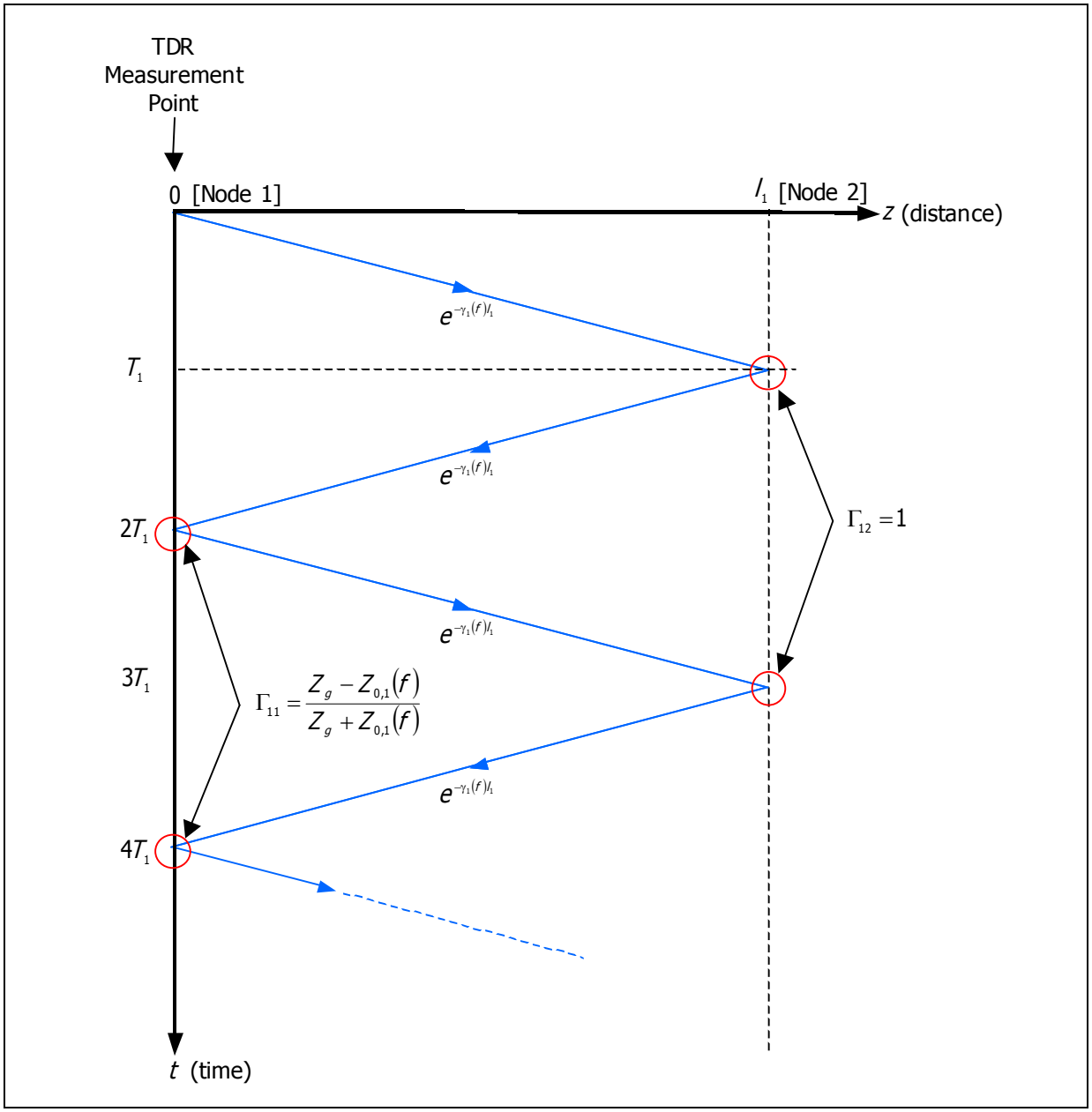

Figure 2-12: Bounce diagram for the local loop configuration in Figure 2-11.

This transmission line signal propagation behavior is also shown by the TDR response, and therefore the bounce diagram correspondingly describes the TDR behavior particularly well. On Figure 2-12, the TDR measurement point is also indicated to make the connection. In essence, every time the signal hits $z=0$, the TDR equipment records the signal. Thus, the overall TDR response is the sum of all reflections returned to the measurement node, or

$$y_{TDR}(t)=\sum_{i=0}^{\infty} y_{ri}(t) \tag{2-18}$$

where $y_{ri}(t)$ is the *i*-th returned reflection. The first one, $y_{r0}(t)$, is the voltage divided version of the excitation pulse $x_{TDR}(t)$. The Fourier spectrum of $y_{r0}(t)$ is

$$Y_{r0}(f)=X(f)\frac{Z_o(f)}{Z_o(f)+Z_g} \tag{2-19}$$

Reverting back to the simple loop in Figure 2-11, the spectra of the following reflections at time NT_1 for all even integers $N\geq 2$ are expressed in terms of the bounce diagram parameters and $Y_{r0}(f)$. The spectra for the first two and *i*-th reflections are expressed as

$$\begin{aligned}
Y_{r1}(f)&=Y_{r0}(f)\mathrm{T}_{11}(f)\Gamma_{11}(f)e^{-2\gamma_1(f)l_1}\\
Y_{r2}(f)&=Y_{r0}(f)\mathrm{T}_{11}(f)\Gamma_{11}^2(f)e^{-4\gamma_1(f)l_1}\\
&\vdots\\
Y_{ri}(f)&=Y_{r0}(f)\mathrm{T}_{11}(f)\Gamma_{11}^i(f)e^{-2i\gamma_1(f)l_1}\\
&\vdots
\end{aligned} \tag{2-20}$$

Since the measurement is taken on the source side of Node 1, the above expressions contain $\mathrm{T}_{11}(f)$.

The TDR response of the loop in Figure 2-11 with a 250-m 24-AWG TP segment is shown in Figure 2-13. The input pulse is the raised-cosine pulse in Figure 2-7. The first three reflections are clearly visible while the rest have been attenuated significantly. However, plotting each reflection separately as in Figure 2-14 allows those attenuated reflections to be observed[1]. Clear attenuation by an order of magnitude is observed by comparing Figure 2-14(c) to Figure 2-14(b) and Figure 2-14(d)

[1] The separation of the pulse is analytically calculated for illustration purposes. TDR equipment cannot perform such an operatio.

to Figure 2-14(c). Furthermore, the illustration indicates that the TP is a lossy and dispersive medium in which the different frequency components of a propagating signal attenuate and travel at different rates.

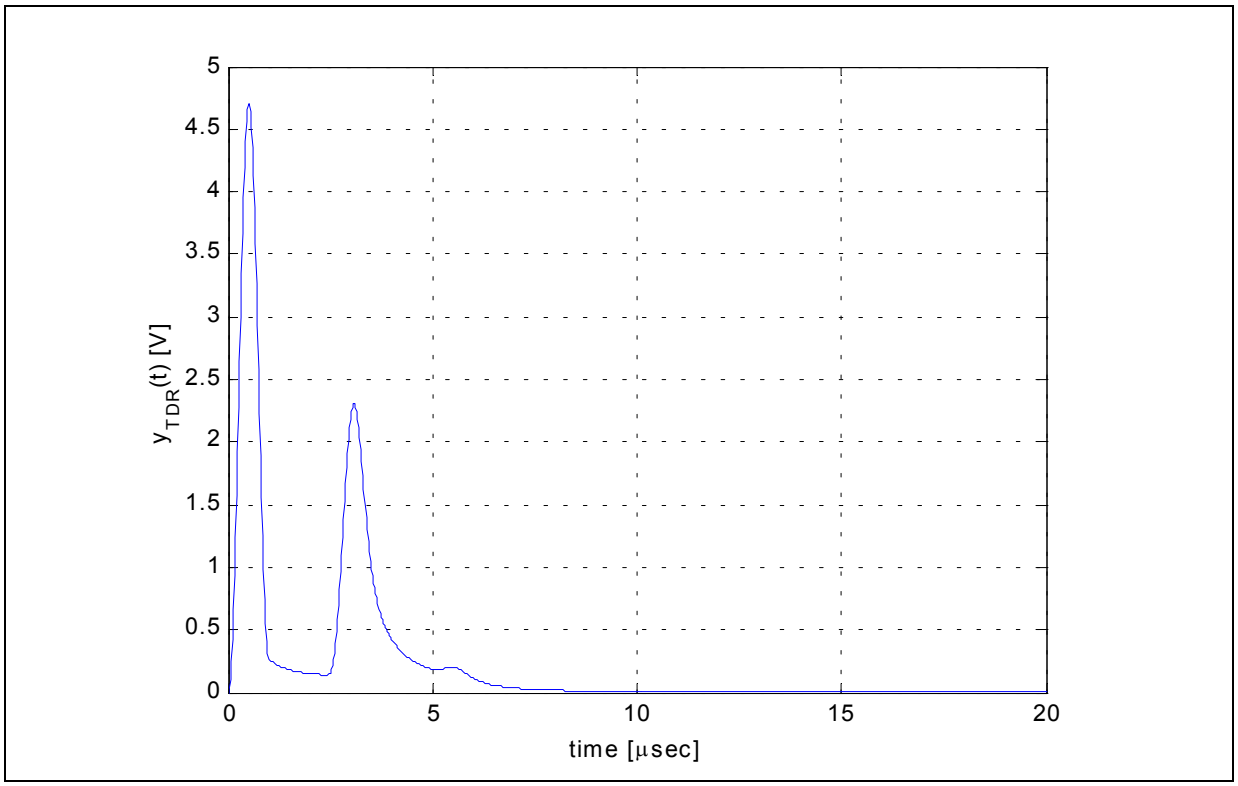

Figure 2-13: The TDR response of Figure 2-11 loop with 250-m 24-AWG TP segment. Input source:10-V 1-μs raised-cosine pulse.

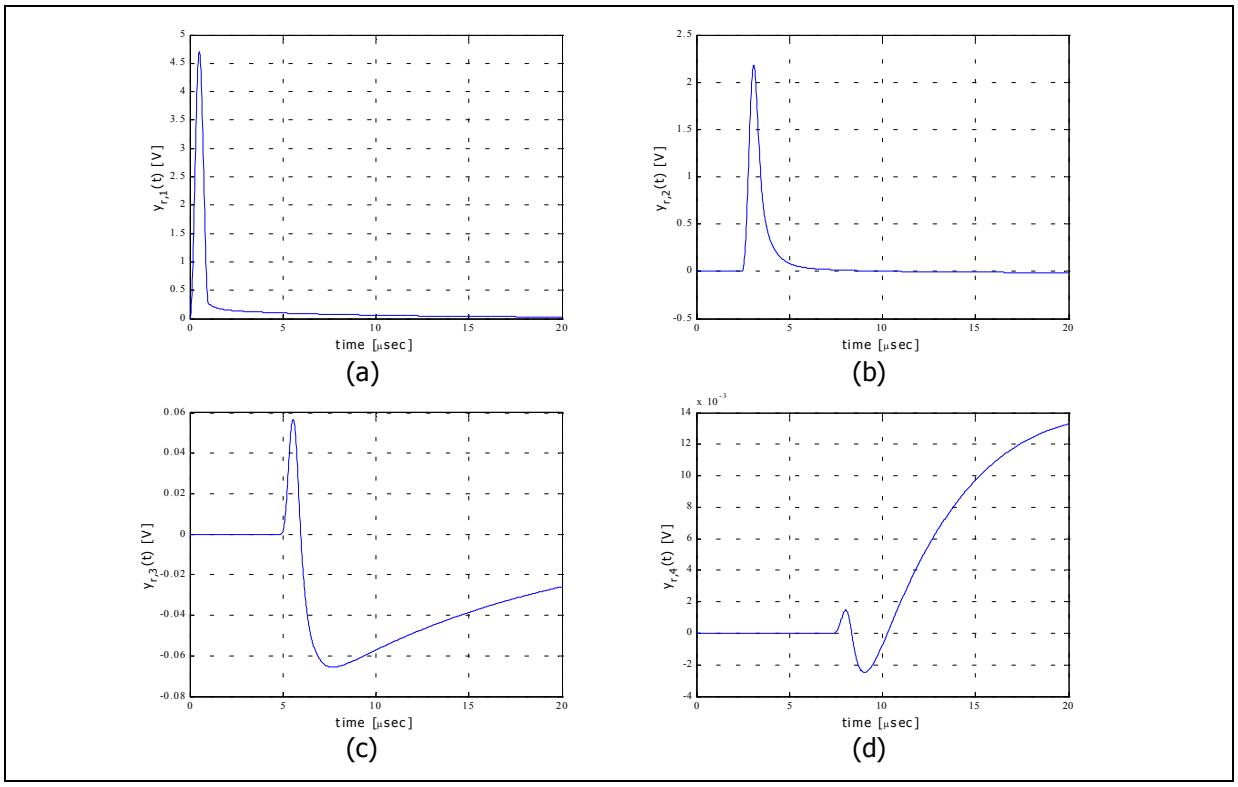

Figure 2-14: First 4 of the TDR reflections within the TDR response in Figure 2-13.

The bounce diagram can be drawn for more complicated loops in the same manner as for the single-segment case. For example, consider the loop in Figure 2-15 with its bounce diagram shown in Figure 2-16. With the addition of a GC discontinuity, both reflections and transmissions at Node 2 are clearly shown. Also, the difference in the TP type will likely cause the signal propagation velocity to vary from Segment 1 to Segment 2 as shown in the bounce diagram.

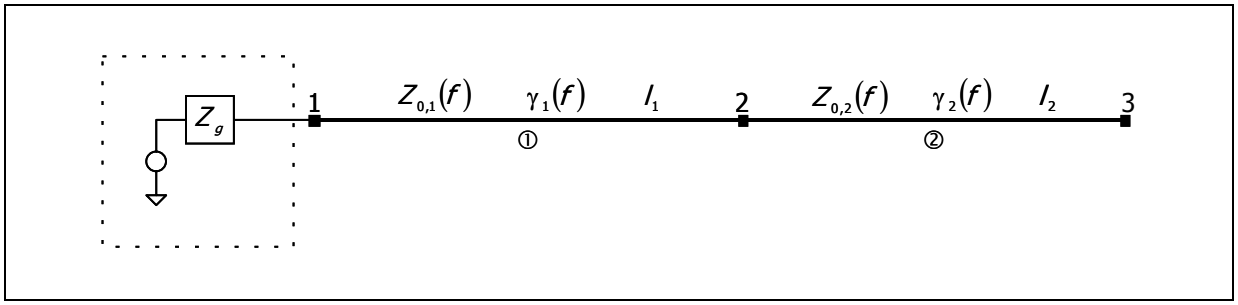

Figure 2-15: Two-segment loop with gauge change.

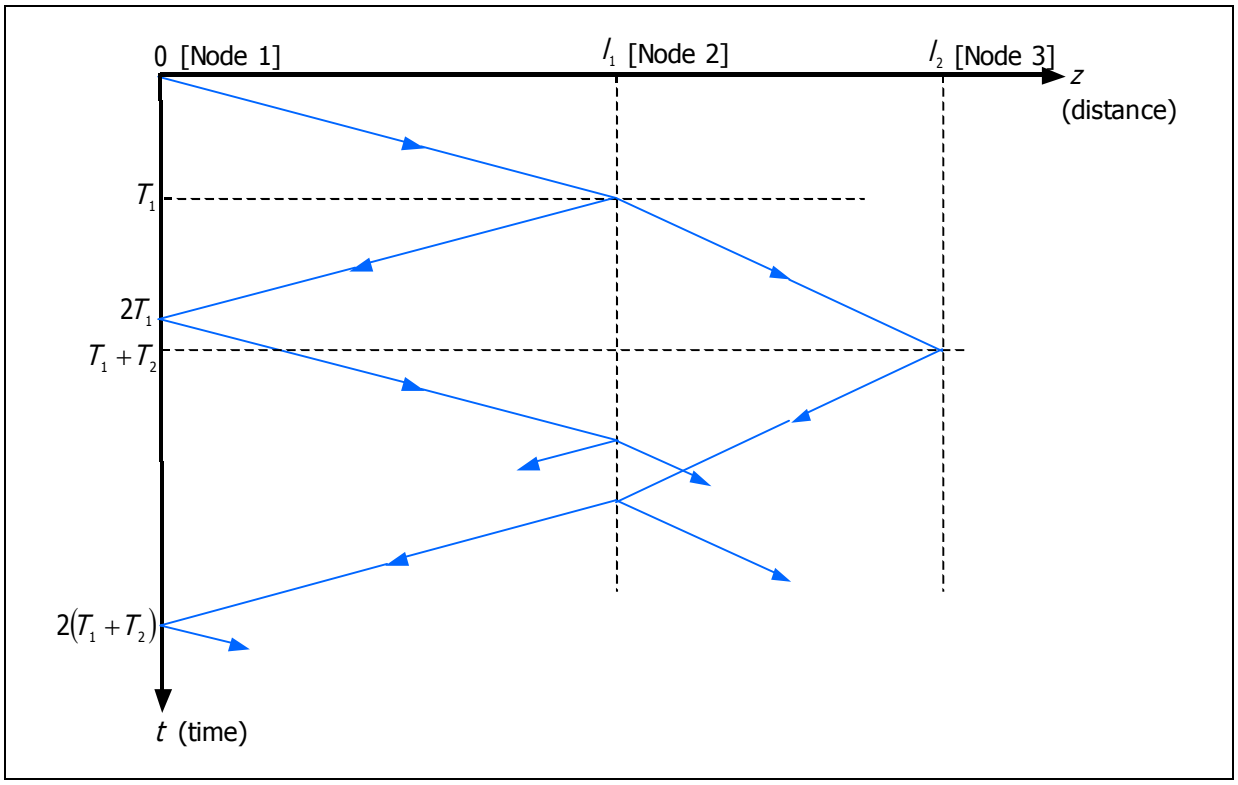

Figure 2-16: Bounce diagram for Figure 2-15.

2.6.2 System Block Diagram

As shown in the previous section, a bounce diagram is an effective tool to visualize the TDR signal propagation process. However, for more complex local loops with multiple segments and bridged taps, drawing bounce diagrams may be challenging. Instead, the signal behavior can be modeled using a block diagram based on the bounce diagram knowledge. The system block diagram can then be divided into separate building blocks; and for a particular local loop structure, appropriate blocks can be interconnected to build the system-level diagram.

Two distinct subsystems play a role in the signal propagation on a local loop: forward (away from source node) and backward (toward source node) propagations over TP segments, and reflection/transmission at loop nodes. Both subsystems are modeled as a multiple-input multiple-output system. The input and output signals of the subsystems are the forward and backward propagations. In terms of those two subsystems, the corresponding block diagrams for the loops in Figure 2-11 and Figure 2-15, and CSA #1 are presented in Figure 2-17.

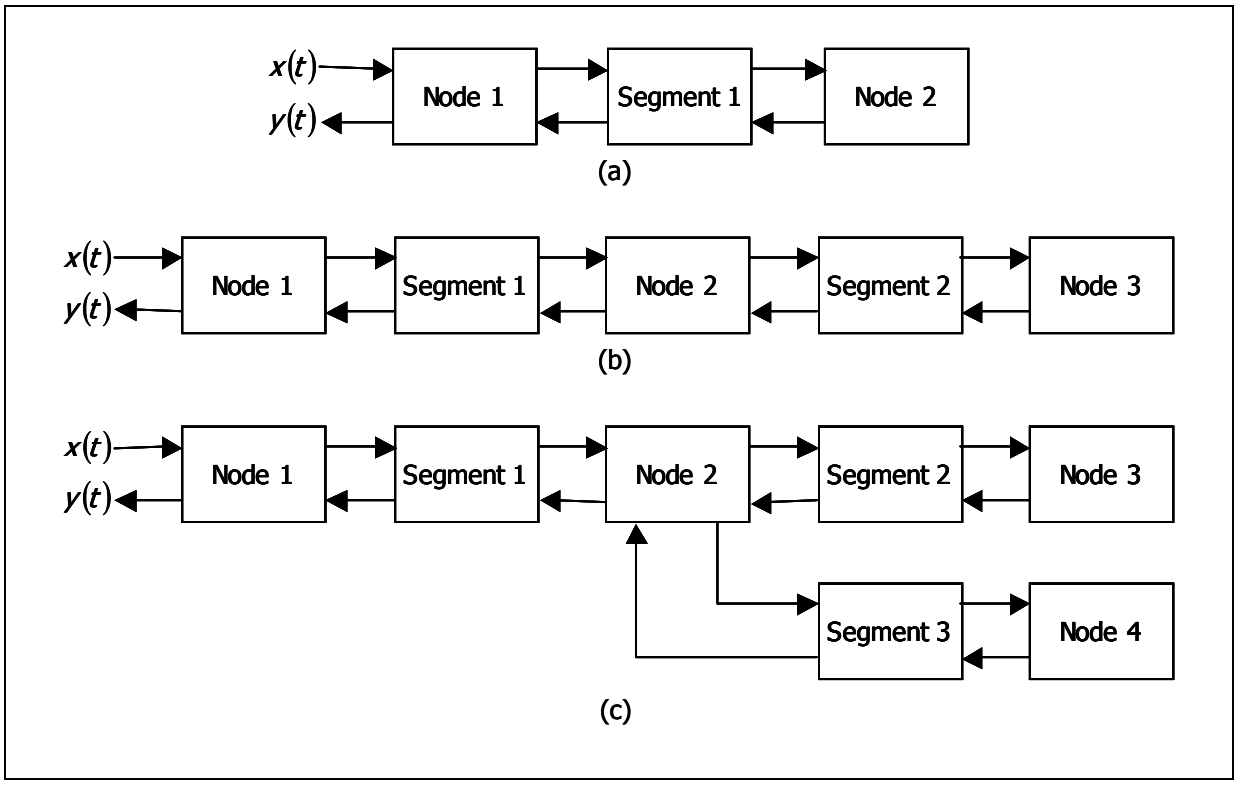

Figure 2-17: Block diagram for Figure 2-11 loop (a), Figure 2-15 loop (b), and CSA #1 loop (c). Segment blocks—propagation blocks. Node blocks—reflection/transmission blocks.

Furthermore, each one of these subsystems can be expressed with a block diagram based on the bounce diagram. Figure 2-18 shows the block diagrams for all of the subsystems. The signal propagation block, Figure 2-18(a), characterizes the signal propagation process through a transmission line (segment blocks in Figure 2-17). The rest correspond to the discontinuity types that are illustrated in Figure 2-10. Figure 2-18(b)–(d) signify the discontinuities at the source node, termination node, GC node, and BT node, respectively.

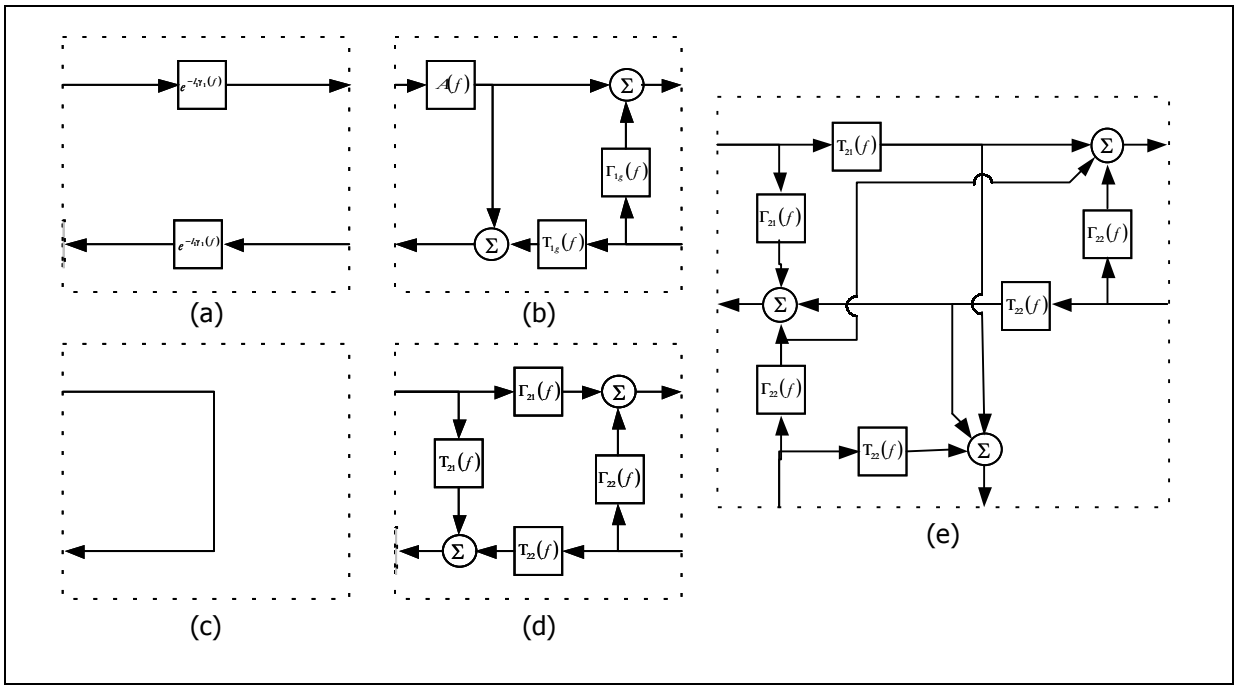

Figure 2-18: System components — propagation (a), source node (b), termination node (c), GC node (d), and BT node (e).

Expanding the subsystems in Figure 2-17(a) yields Figure 2-19. Each path from $x(t)$ to $y(t)$ corresponds to a reflection seen in the TDR response and is also equivalent to the bounce diagram signal flow. This interpretation allows complex loops to be represented in a systematic way without losing the behavior of the TDR response gained from the bounce diagram.

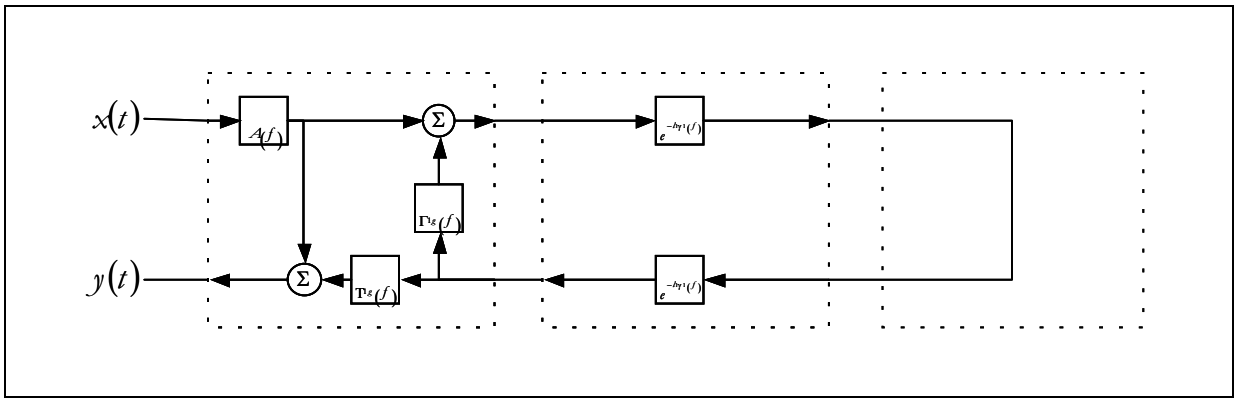

Figure 2-19: Complete block diagram for measurement of Figure 2-11 loop.

2.7 Summary

This chapter establishes two important methods that are used in the TP subscriber loop identification process. The first is the modeling of the measurement setup as an LTI system, and the second is the breakdown of the overall system into meaningful subsystems based on bounce diagrams. With the LTI system representation of the measurement process, most measurement types can be simulated with ease by convolution and a pair of DFT and IDFT operations.

The modeling of the measurement setup requires a twisted-pair characteristic model and a local loop structural model. The former is based on the VT-TDL model, and the parameters for potential TP types are stored in a database. The local loop structural models are modeled with graphs. With these models, the measurement setup is modeled as a voltage divider circuit with the loop's equivalent impedance and the source impedance. The input and output of the circuit are viewed as the input and output of an LTI system, and its frequency response is easily obtained in terms of source and loop equivalent impedances.

The transient behavior seen in the TDR measurement is indicative of the structure of the LUI. The bounce diagram, a technique used in transmission line analysis, describes the time-domain responses of the system as a sum of reflections returning from the loop discontinuities. Based on this notion, (modular) system block diagrams are derived to describe the loop as an LTI system while maintaining the intuition gained from the bounce diagram study.